Hindawi
Mathematical Problems in Engineering
Volume 2018, Article ID 8359145, 12 pages
https://doi.org/10.1155/2018/8359145

Research Article

Shock Wave Characteristics of Hydraulic Shock Wave Simulator with Variable Damping

Xiaoqiu Xu,[1,2] **Zhongwen Wang**,[2] **Junwei Han**,[1] **and Dacheng Cong**[1]

[1]*School of Mechatronics Engineering, Harbin Institute of Technology, Harbin 15000, China*
[2]*Department of Mechanics, Harbin University of Science and Technology, Rongcheng Campus, Rongcheng 264300, China*

Correspondence should be addressed to Xiaoqiu Xu; 13b908020@hit.edu.cn

Received 5 January 2018; Revised 2 April 2018; Accepted 4 December 2018; Published 30 December 2018

Academic Editor: Yannis Dimakopoulos

For simulating the shock wave with high peak force in a short duration, a novel variable damping hydraulic shock wave simulator was developed, and it was used for simulating the cannon recoil motion. The working principle of this simulator was explained with the assistance of established mathematical model and the flow behavior in damping channel was analyzed. The shock wave characteristics curves were obtained by using the numerical computation method. The results showed that the shock wave characteristics were directly related to the sectional area of the damping channel and the damping fluid medium characteristic; the shock wave curve can be simulated by adjusting the variable damping parameters. The computational results agreed well with the theory analysis, which meant that the proposed mathematical model can be used for supplying theoretical references for the cannon recoil motion in artillery fire shock simulation test.

1. Introduction

Since the 1950s, equivalent reliable artillery simulation test method had been initially developed, for example, a shock simulation tester equipped with a hydraulic shock cylinder was explored by US researchers [1, 2]. The typical experimental methods of simulating the shock also included gas guns, resonant fixtures, drop towers, and Hopkinson/Kolsky bars [3–6], and the blast simulator had proven to be effective in simulating the shock load [7]. Because of the high peak acceleration and short pulse duration, it was hard to obtain the shock levels experienced by various defense-related structure and mechanical components in practice. However, hydraulic actuators were reported in simulating the explosion shock in previous literatures, and the system used hydraulic actuators to fire a piston mounted with various impact materials at high velocity; the results showed that this shock simulator had proven to be effective for simulating explosive shock force [8–10]. The distribution of blast-like pressures had been studied using the shock simulator in University of California, and the bladder material, use of baffles, and strapping ways were varied along with the input parameters such as shock velocity and shock mass geometry [11]. Freidenberg A and Lee C W. investigated the impact response of elastomer materials and the response was used to induce impulsive load like shock load [12]. The shock simulator in University of California, San Diego, was an appropriate tool for developing full-scale test of shock effects on the structures or the mechanical components, and this shock simulator used high velocity hydraulic actuators to impact the designed modules towards the specimen [13].

As the fast development of computational simulation, numerical simulation was gradually introduced in fire shock simulation tester. Based on the theory of classical internal ballistics and systematic dynamic, numerical simulation model of the artillery recoil system simulator was built by Yao et al. [14]. Considering structure parameters and the load conditions of DS-II artillery recoil system, the further optimization model was developed by Xu et al. [15]. For investigating the stereotype of ground artillery tester, a virtual recoil tester was developed by Di and Liu using MSC. ADAMS. Applying homogeneous experiment design, the simulation of dynamic recoil process was achieved and influence of shock parameters was studied using the software

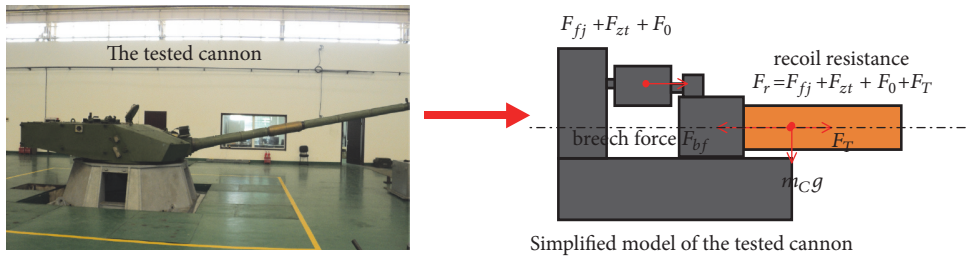

Figure 1: Force analysis of the cannon recoil subsystem.

Matlab [16, 17]. The constitutive models and optimization design of the rubber wave simulators were built by Yang et al. [18–22]. The reports showed that the method using a mass block with high speed impacting cannon muzzle to simulate cannon firing process was proved to be a feasible recoil simulation test method [23, 24].

It was obvious that shock simulation tests and the simulation method were necessary in various fields from previous literatures, and the shock wave simulator played an important role in energy transferring and conversion. And in hydraulic shock simulator, shock wave characteristics were analyzed by Jiao and Wang using shock test machine, including the influence of the annular gap, the diameter of the orifice pore, and shock wave under different velocities [25]. Shock simulator models evaluation and nonexhaustive overview of shock simulator models were presented by Stefaan Duym and Randy Stiens [26]. Hydraulic shock simulator valve behavior was analyzed by Shams M and Ebrahimi R using the method of CFD-FEA [27]. The mathematical model of fluid viscous shock simulator used in the shock test was derived by Jia and Du [28]. Considering a simple annular orifice, a new model for nonlinear viscous fluid dampers used in the shock or damper fields was proposed by Hou C Y and its fluid dynamics behavior and shear-thinning effects were analyzed [29–31]. Accounting for effects of shear-thinning and viscoelasticity, the scholars A Syrakos, Y Dimakopoulos, and J Tsamopoulos used different rheological models to describe the behavior of the fluid, which revealed that the damper behavior was related to the fluid rheology. In addition, and full two-dimensional (axisymmetric) simulations of the flow in a damper were also performed which models the fluid employing a viscoelastic constitutive equation [32].

Therefore, the shock wave characteristics of novel shock wave simulator used in the simulation of the cannon recoil motion were discussed in this paper. The working principle of this simulator was explained, the mathematical model was established, and the flow behavior in damping channel was analyzed. In additions, the serious shock wave curves were simulated by adjusting the fluid damping parameters and the shock velocity as well as the tested mass.

2. Shock Principle and Structure Description

2.1. Shock Principle. Based on the working principle of the live firing muzzle shock test, the breech force that acts on the breech axis in live firing is an active force that drives the cannon recoil motion, which reaches $10^7 N$, and the whole process just requires (5-11)ms; this process belongs to an instant strong shock. The sketch of the cannon force analysis is shown in Figure 1.

For the cannon, the force balance equation is simply written as

$$m_c \frac{d^2 x_1}{dt^2} = F_{bf} - F_r \tag{1}$$

where m_c is the mass of cannon recoil parts; x_1 is the recoil displacement; t is the recoil time; F_{bf} is the breech force; F_r is the recoil resistance. In a shock simulation test, an active force that drives artillery recoil motion is F_S generated by the mass block impacting the cannon muzzle under a high velocity.

$$m_c \frac{d^2 x_1}{dt^2} = F_S - F_r \tag{2}$$

where F_S is the shock force; the alternative model of breech force, that the shock force F_S replaces the breech force F_{bf}, plays a similar explosive and promoting role for propellant burning. Therefore, for making the shock simulation test be of higher precision, we need to design suitable shock parameters and structure forms to ensure the equivalence between the shock force and the breech force. Therefore, for making sure that dynamic behavior of the cannon shock simulation test can be similar to the live firing, similar simulation method is chosen, which could generate instant strong shock effect.

The elastic material such as the rubber pads was used as the convenient shock wave simulator, which has three disadvantages. Firstly, the shock mass or shock severity was limited due to the strength of the simulator, and it cannot satisfy all the requirements of modern aero, military, and marine industries. Figure 2 showed the shock simulation tester with a rubber shock simulator; secondly, the reproduction depended on the characteristic of the shock simulator. Because the permanent deformation usually occurred after several impacts, the shock wave form cannot repeat accurately; thirdly, the conventional shock simulation test table can only generate regular shock wave which was usually true in the buffer or damper systems, but in the shock environment, which presented high shock force, short shock time and steep shape.

Shock and restoration process is described as Figure 3. The shock wave simulator is accelerated by the velocity generator and then impacts the cannon muzzle, after a shock

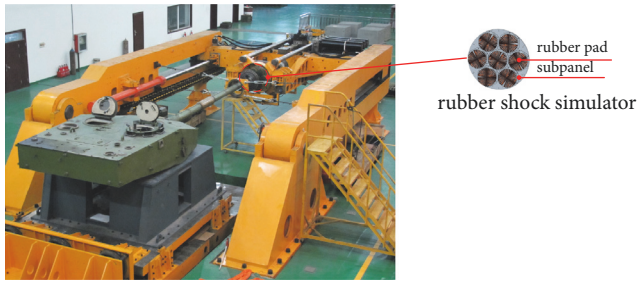

Figure 2: Shock simulation test table with rubber shock simulator.

process is finished, the shock wave simulator restates. After the above steps, a shock test is finished, repeating the above process to carry on many experiments. In a shock simulation test, the shock wave simulator is a key component which played an important role of the shock energy transfer and conversion.

The traditional rubber shock simulator is usually used for the regular shock wave reappearance such as a half-sine shock wave. However, the practical cannon shock force wave that simulates the breech force has the characteristic of steep prepeak and gentle postpeak relatively (dotted line shown as in Figure 12); the traditional rubber wave simulator is not fit for the simulation. However, the hydraulic shock wave simulator can also be developed to be a shock wave programmer, and because the kinetic energy can be absorbed simultaneously, the input velocity can go to zero in the end. Besides, by adjusting the fluid damping passage, the shock wave characteristic can be regulated, and the effects of structure parameters and shock parameters on dynamics and behavior have drawn attentions for hydraulic shock wave simulator. Therefore, for simulating the practical shock force wave, a new idea about variable damping hydraulic shock wave simulator is proposed based on the hydraulic buffering technology.

2.2. Structure Description. The shock simulation system adopts the momentum transfer principle, a shock wave simulator with a certain velocity transfers the momentum into the cannon barrel during the shock process, and the large shock force is formed on the cannon barrel; in addition, the various shock force wave can be achieved by adjusting the damping and rigidity of the shock wave simulator. The structure sketch of the high-power hydraulic shock wave simulator is shown as Figure 4; the hydraulic oil is filled in the shock wave simulator. The inner diameter of the fixed block is 436mm, and its initial length is 120mm; the inner diameter of the moving block is 310 mm, and its initial length is 80mm; there are variable throttle gap widths in the throttle passage. During a shock process, when an external shock force is applied to the left of the shock wave simulator, the moving block moves towards the right; the oil in the right fixed block chamber is compressed and flows through the throttle gap into the left chamber (as the red arrow shown in Figure 4).

In this process, the corresponding damping force is raised to balance the external shock force.

3. Mathematical Models

The sketch of the whole model is shown in Figure 5. In the figure, the model consists of three subsystems, the left one is the recoil subsystem, the right one is the damping subsystem including a damper, and the middle one is the impact subsystem.

In the high-power shock simulation test, the whole simulation process could be divided into two stages. The shock process is the first stage, in this process, the rubber pad that is located on the pounding head of a variable damping hydraulic shock wave simulator collides with the canon muzzle and supplies the velocity to the cannon barrel and accelerates the canon barrel including recoil buffer device and the cannon suffers the shock force from the shock subsystem and the resistance from the recoil subsystem. In the second motion process, the moving block part will be braked by the damping part of the novel variable damping hydraulic shock wave simulator.

In the simulation process, variable damping shock wave simulator with certain initial velocity impacts the static tested cannon barrel, the moving cylinder block and the tested cannon barrel accelerate with common velocity during the impact process, the fixed cylinder block decelerates, and the relative velocity between the moving cylinder block and the fixed cylinder block is generated.

And the fluid in the fixed cylinder block is compressed to generate the damping force during the fluid damping process, and this damping force simulates the shock force wave. The shock simulation wave is finished when the relative velocity is zero.

3.1. Model of the Recoil Subsystem and the Force Analysis. The breech force driving the recoil parts to recoil is the active force when the cannon recoils, and the cannon is stopped to recoil because of the recoil resistance; the relative relationship between the recoil resistance and the active force causes the velocity changes and the acceleration changes [33]. This recoil subsystem force analysis is shown in Figure 2. The differential equation of the cannon recoil motion is built using the Newton's second law of motion (when the canon firing angle is equal to 0°).

$$m_C \frac{d^2 x_1}{dt^2} = m_C \frac{dv_1}{dt} = F_{bf} - F_{fj} - F_{zt} - (F_0 + F_T) \quad (3)$$

where m_C is the mass of the recoil parts, x_1 is the recoil distance, v_1 is the recoil velocity, F_{fj} is the recuperator force, F_{zt} is the recoil brake force, and $(F_0 + F_T)$ is the frictions generated on the cradle guide rail and seal application. The definition of the cannon recoil resistance F_r is written as $F_r = F_{fj} + F_{zt} + F_0 + F_T$, so the differential equation of the cannon recoil motion is simplified as

$$m_C \frac{d^2 x_1}{dt^2} = m_C \frac{dv_1}{dt} = F_{bf} - F_r \quad (4)$$

The recoil motion can be divided into the following periods. The recoil active force F_{bf} is much larger than the recoil resistance F_r, the acceleration is positive in this period if

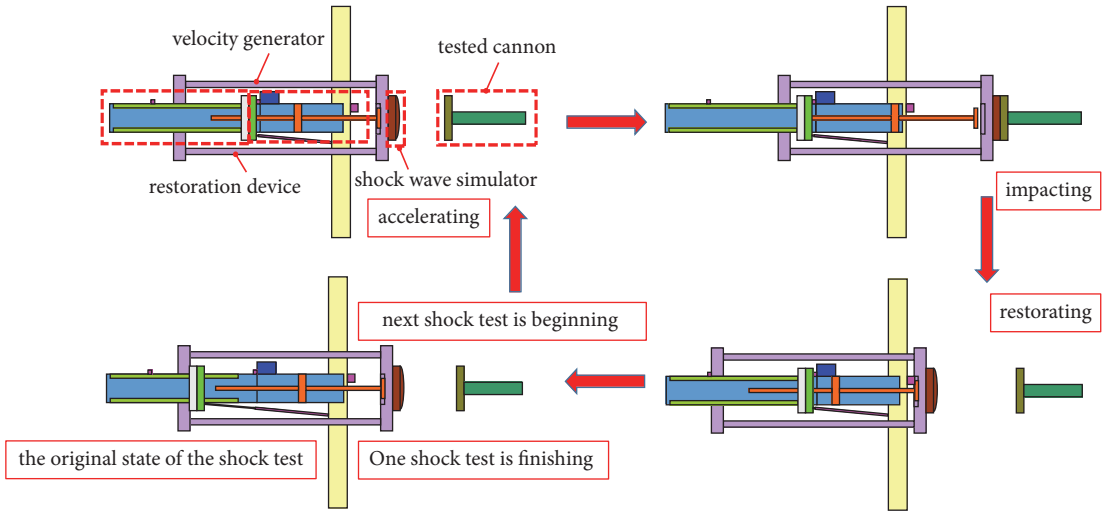

Figure 3: Simplified sketch of the shock and restoration process.

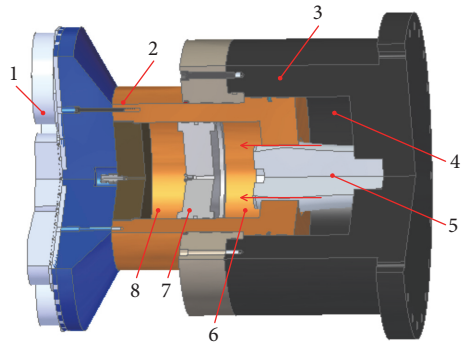

Figure 4: Structure stretch of the hydraulic shock wave simulator. 1: elastic element, 2: moving cylinder block, 3: fixed cylinder block, 4: high pressure cavity, 5: throttle core shaft, 6: low pressure cavity, 7: isolation piston, and 8: nitrogen gas cavity.

setting that the direction of the breech force F_{bf} is positive, the velocity increases from zero sharply, one moment exists after that, and at the moment, the acceleration is zero, $F_{bf} = F_r$, the recoil resistance is the maximum value at the moment in the whole recoil process, and the recoil velocity is maximum. The recoil motion is going on after that, the breech force decreases, the recoil active force F_{bf} is smaller than recoil resistance F_r, the recoil velocity decreases, and the recoil motion stops when the velocity v_1 is zero.

The recuperator force can be expressed as below in a recoil process:

$$F_{fj} = 50000 \times \left(\frac{2.15}{2.15 - x_1}\right)^{1.3} \tag{5}$$

where x_1 is the displacement of the cannon recoil part. The recuperator force is a function related to the canon recoil displacement. The recuperator force could be expressed as below in recoil process.

$$F_{zt} = \left(1800 \times \frac{150 + a_x}{{a_x}^2} + 130\right)\left(\frac{dx_1}{dt}\right)^2 \tag{6}$$

where a_x is equivalent area of recoil brake vintage and dx_1/dt is the canon recoil velocity.

$$a_x = \left(23 - \frac{\pi}{4}{d_x}^2\right) \tag{7}$$

where d_x is throttling bar diameter. Although the corresponding throttling bar diameters under different recoil displacement are different, the throttling bar diameter keeps constant.

$$F_{zt} = 1580\frac{dx_1}{dt} \tag{8}$$

The recoil brake force is a function related to the canon recoil velocity. The constant friction F_f could be expressed as follows:

$$F_f = f_1 mg + F_0 \tag{9}$$

where f_1 is the friction coefficient between canon recoil and cradle and F_0 is the friction generated by plug component of counter recoil mechanism, which is composed by two parts.

$$F_0 = F_{01} + F_{02} \tag{10}$$

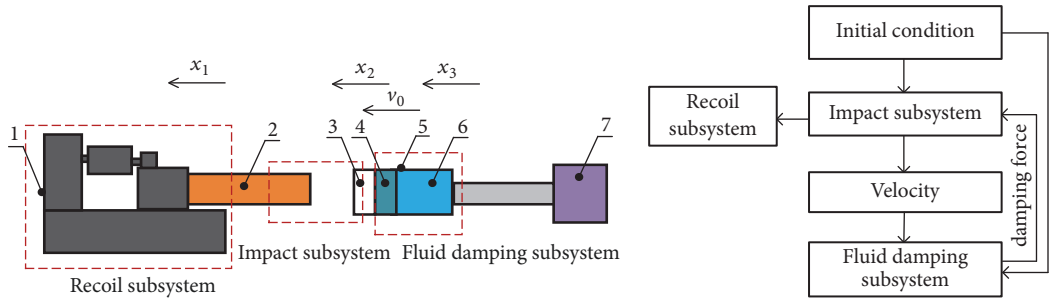

(a) Coupled system sketch (b) Coupled system diagram

FIGURE 5: Coupled models for the shock simulation system. 1: recoil mechanism, 2: the cannon barrel, 3: elastic element, 4: moving cylinder block, 5: variable damping shock wave simulator, 6: fixed cylinder block, and 7: velocity generator.

where F_{01} is the friction generated by plug component in recuperator and F_{02} is the friction generated by plug component in the recoil brake. When the canon firing angle keeps constant, the constant friction can be seen as a constant value. $F_f = 10500N$ when the canon firing angle is equal to 0°.

In conclusions, the force balance equation of the shocked canon is expressed as below when firing angle is 0°.

$$\begin{aligned} m_C \frac{d^2x_1}{dt^2} &= F_S - F_{fj} - F_{zt} - F_f \\ &= F_S - 50000 \times \left(\frac{2.15}{2.15 - x_1}\right)^{1.3} - 1580\frac{dx_1}{dt} \\ &\quad - 10500 \end{aligned} \tag{11}$$

where d^2x_1/dt^2 is the recoil acceleration.

3.2. Model of the Impact Subsystem and the Force Analysis. The mass of the moving cylinder block is assumed as m_v, elastic element locates between the moving cylinder block and the tested object, and F_n is assumed as the normal contact force at the position of the contact point. Based on the force analysis of the tested object m_C in the impact subsystem, differential equation of motion is obtained as

$$\begin{aligned} m_C \frac{d^2x_1}{dt^2} &= F_n - 50000 \times \left(\frac{2.15}{2.15 - x_1}\right)^{1.3} - 1580\frac{dx_1}{dt} \\ &\quad - 10500 \end{aligned} \tag{12}$$

Based on the force analysis of the moving cylinder block m_v in the impact subsystem, differential equation of motion is obtained as

$$m_v \frac{d^2x_2}{dt^2} = -F_n + F_{DM} \tag{13}$$

where F_{DM} is the output damper force of the variable damping hydraulic shock wave simulator.

3.3. Model of the Fluid Damping Subsystem and Flow Behavior Analysis Using the Variable Damping Gap. The novel high-power hydraulic shock wave simulator adopts novel variable damping structural forms, and the relative motion between the moving cylinder block and the fixed cylinder block compresses the fluid in the cylinder to export the corresponding damping force.

Based on the force analysis of the fixed cylinder block in the fluid damper subsystem, the differential equation of the motion is obtained as

$$m_f \frac{d^2x_3}{dt^2} = -F_{DM} \tag{14}$$

Because the damping gap width is much smaller than the inner diameter of the cylinder, the flow in damping gap can be simplified as Couette-Poiseuille flow in the parallel plates, consisting of one velocity component. The flow behavior of the Couette-Poiseuille flow of the Newtonian fluid and non-Newtonian fluid is derived in parallel plates using Navier-Stokes equation [34, 35].

3.3.1. Flow Behavior Analysis of Couette-Poiseuille Flow of the Newtonian Fluid in the Damping Passage. Assume that the distance between two infinite parallel plates is h, shown as Figure 6, X-axis coincides with the center line of the two plates, Y-axis is perpendicular to the paper face, Z-axis is the height between the two plates, and the fluid flows along X-axis under the influence of the pressure gradient.

According to the momentum conservation laws, the fluid flow satisfies the Navier-Stokes equation.

$$\rho\frac{\partial V}{\partial t} + \rho\,(V \bullet \nabla)\,V = \rho f - \nabla p + \frac{1}{3}\eta\nabla\,(\nabla \bullet V) + \eta\nabla^2 V \tag{15}$$

where ρ is the fluid density, V is the per unit velocity vector, f is per unit mass force, p is the pressure, η is the kinetic viscosity, and ∇^2 is the Laplace operator, that is $\nabla^2 = \partial^2/\partial x^2 + \partial^2/\partial y^2 + \partial^2/\partial z^2$. The left side of (15) is the acceleration of per unit fluid, which is fluid inertia force. The right side of the first item is the force on per unit fluid such as gravity related to the mass.

The second item represents the pressure gradient on per unit fluid; the third item and fourth item represent the viscosity force on per unit fluid; where the third item is the viscous expansion stress, the fourth item is the viscous deformation stress. Equation (15) is applied in Poiseuille flow

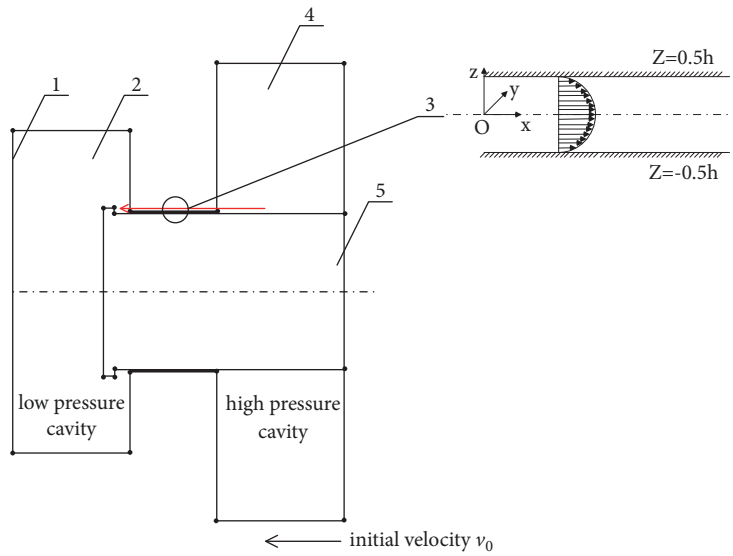

Figure 6: Simplified fluid model of hydraulic shock wave simulator. 1: isolation piston, 2: moving cylinder block, 3: throttle gap, 4: fixed cylinder block, and 5: throttle core shaft.

in two parallel plates; firstly, assume that the fluid flow is stable laminar, f in (15); secondly, the flow is viscosity fluid; viscous force is dominant; besides, the mass force and inertia force are both ignored; therefore, the second item of (15) left side is zero, f is also zero; in addition, assume that the fluid is incompressible fluid, the third item is equal to zero, so the equation can be simplified as

$$-\nabla p + \eta \nabla^2 V = 0 \tag{16}$$

Because of the only fluid motion along X-axis, (16) can be expressed as

$$-\frac{dp}{dx} + \eta \frac{d^2 v_x}{dz^2} = 0 \tag{17}$$

Take a finite length L whose pressure drop is Δp along X-axis.

$$\frac{dp}{dx} = -\frac{\Delta p}{L} \tag{18}$$

Therefore, (17) can be expressed as

$$\frac{d^2 v_x}{dz^2} = -\frac{\Delta p}{\eta L} \tag{19}$$

The wall meets the no-slip condition; the corresponding boundary conditions are written as $z = 0.5h$, $v_x = 0$; $z = -0.5h$, and $v_x = 0$. The velocity distribution of the Newtonian fluid is obtained by solving the equations; the Newtonian fluid viscosity η is assumed as η_0 which is constant.

The integration of (19) is written as

$$\frac{dv_x}{dz} = -\frac{\Delta p}{\eta_0 L} z + C_1 \tag{20}$$

The integration of (20) along Z direction is written as

$$v_x = -\frac{\Delta p}{2\eta_0 L} z^2 + C_1 z + C_2 \tag{21}$$

The boundary condition is plugged into (20), $C_1 = 0$ and $C_2 = (\Delta p / 2\eta_0 L)(h/2)^2$ are obtained, and the two coefficients are plugged into (21); the velocity distribution of Newtonian fluid is obtained as follows:

$$v_x = \frac{h^2 \Delta p}{2\eta_0 L} \left[\frac{1}{4} - \left(\frac{z}{h} \right)^2 \right] \tag{22}$$

The velocity distribution of Newtonian fluid Poiseuiue flow in parallel plates is standard parabolic; the wall velocity is zero; the maximum velocity appears at the position $z = 0$ in the center of the two plates.

$$v_x^{\max} = \frac{h^2 \Delta p}{8\eta_0 L} \tag{23}$$

Corresponding shear strain rate is written as

$$\dot{\gamma}_{zx} = \frac{dv_x}{dz} = -\frac{\Delta p}{\eta_0 L} z \tag{24}$$

Shear stress distribution is written as

$$\tau_{zx} = \eta \dot{\gamma}_{zx} = -\frac{\Delta p}{L} z \tag{25}$$

ΔP is expressed as the pressure gradient instead of $\Delta p / L$; (25) is written as

$$\tau_{zx} = -\Delta P z \tag{26}$$

Through the analysis, we could draw a conclusion that the shear stress on Newtonian fluid is zero at the position $z = 0$ in the center of the two parallel plates, and the maximum shear stress is $|0.5h\Delta P|$which appears on the wall; the shear strain rate also changes with the shear stress changes, and its maximum value is $|0.5h\Delta P|/\eta_0$.

3.3.2. Flow Behavior Analysis of Couette-Poiseuille Flow of Non-Newtonian Fluid in the Damping Passage. Derivation process of the motion equation of the non-Newtonian fluid is the same as that of the Newtonian fluid; the motion equation of non-Newtonian fluid in two parallel plates is directly concluded as

$$-\frac{dp}{dx}+\frac{d\tau_{zx}}{dz}=0 \tag{27}$$

The item dp/dx is placed by $-\Delta p/L$; (27) could be concluded as

$$\frac{d\tau_{zx}}{dz}=-\frac{\Delta p}{L} \tag{28}$$

For the simplified calculation, power-law model is used to solve it, and constitutive equation of power-law fluid is written as

$$\tau_{zx}=\eta\left(\dot{\gamma}_{zx}\right)^{n} \tag{29}$$

where n is the flow index and corresponding boundary conditions are written as $z=0, \tau_{zx}=0$ and $z=\pm h/2, v_x=0$.

The velocity distribution of the non-Newtonian fluid is solved; (28) is written as below by the once integration.

$$\tau_{zx}=-\frac{\Delta p}{L}z+C_1 \tag{30}$$

It is concluded that $C_1=0$ according to the boundary conditions.

$$\tau_{zx}=-\frac{\Delta p}{L}z \tag{31}$$

Equation (31) is plugged into (29); the velocity gradient represents the shear strain rate.

$$\dot{\gamma}_{zx}=\frac{dv_x}{dz}=\left(\frac{\tau_{zx}}{\eta}\right)^{1/n}=-\left(\frac{\Delta p}{\eta L}\right)^{1/n}z^{1/n} \tag{32}$$

Equation (32) is written as follows by the once integration:

$$v_x=-\frac{n}{n+1}\left(\frac{\Delta p}{\eta L}\right)^{1/n}|z|^{(n+1)/n}+C \tag{33}$$

Using the boundary conditions,

$$C=\frac{n}{n+1}\left(\frac{\Delta p}{\eta L}\right)^{1/n}\left(\frac{h}{2}\right)^{(n+1)/n} \tag{34}$$

Equation (34) is plugged into (33), the velocity distribution of Couette-Poiseuille flow of the power-law fluid in two parallel plates is expressed as

$$\begin{aligned}v_x&=\frac{n}{n+1}\left(\frac{\Delta p}{\eta L}\right)^{1/n}\left(\frac{h}{2}\right)^{(n+1)/n}-\frac{n}{n+1}\left(\frac{\Delta p}{\eta L}\right)^{1/n}\\&\cdot|z|^{(n+1)/n}=\frac{n}{n+1}h^{(n+1)/n}\left(\frac{\Delta p}{\eta L}\right)^{1/n}\\&\cdot\left[\left(\frac{1}{2}\right)^{(n+1)/n}-\left(\frac{|z|}{h}\right)^{(n+1)/n}\right]\end{aligned} \tag{35}$$

We could draw a conclusion that the velocity distribution of Couette-Poiseuille flow of power-law fluid in two parallel plates has deviated from standard parabolic-shape. The velocity is zero at the position $z=\pm h/2$ on the wall, and the maximum velocity appears at the position$z=0$ of the center of the two plates.

$$v_x^{\max}=\frac{n}{n+1}\left(\frac{h}{2}\right)^{(n+1)/n}\left(\frac{\Delta p}{\eta L}\right)^{1/n} \tag{36}$$

The corresponding shear strain rate is written as

$$\dot{\gamma}_{zx}=\frac{dv_x}{dz}=-h^{1/n}\left(\frac{\Delta p}{\eta L}\right)^{1/n}\left(\frac{|z|}{h}\right)^{1/n} \tag{37}$$

The shear stress distribution is written as

$$\tau_{zx}=\eta\left(\dot{\gamma}_{zx}\right)^{n}=-\frac{\Delta p}{L}|z| \tag{38}$$

where ΔP is used to represent pressure gradient instead of $\Delta p/L$, it is concluded that shear stress distribution of non-Newtonian fluid is same as that of Newtonian fluid in Couette-Poiseuille flow in parallel plates. For non-Newtonian fluid, the strain stress is zero at the position $z=0$ in the center of two plates, and the maximum shear stress is $|0.5h\Delta P|$ that appeared at the position $z=\pm h/2$ on the wall. The changes of shear strain rate are consistent with shear stress and the maximum shear strain rate is $(|\Delta 0.5hP|/\eta)^{1/n}$.

3.3.3. Derivation of the Fluid Output Damping Force. For the fluid damping passage, Reynolds number is much smaller than critical Reynolds number; therefore, the flow could be simplified as the laminar flow, because the flow velocity shows the symmetric distribution, whose symmetry plane locates in the center plane of the damping clearance, the flow through the clearance could be calculated through dividing into two parts, and the two parts Q_1 and Q_2 can be presented as follows:

$$Q_1=\int_{-h/2}^{0}v_x\cdot 2\pi\left(R_{piston}-z\right)dz \tag{39}$$

$$Q_2=\int_{0}^{h/2}v_x\cdot 2\pi\left(R_{piston}+\frac{h}{2}+z\right)dz \tag{40}$$

where R_{piston} is the piston radius. The total flow through damping gap is expressed as

$$Q=Q_1+Q_2 \tag{41}$$

Because of the continuity equation, the flow through damping gap is equal to the flow of the random section.

$$Q=\left(A_{cylinder}-A_{rod}\right)\cdot V \tag{42}$$

where $A_{cylinder}$ is the cross-sectional area of the cylinder block, A_{rod} is the cross-sectional area of the piston rod, and V is the motion velocity of the piston. Equation (41) is plugged into the equation (42).

$$\Delta p = \frac{2\eta L \cdot \left[\left(R_{cylinder}^2 - r_{rod}^2\right)(n+1)\right]}{\left\{2n\left[((2n+2)/(2n+1))\, R_{piston} \cdot (h/2)^{1/n+2} + (h/2)^{1/n+3} \cdot \left(11n^2+12n+3\right)/(2n+1)(3n+1)\right]\right\}^n} \cdot V^n \tag{43}$$

Hence, output damping force could be expressed as

$$F_{DM} = \frac{2\pi\eta L \cdot \left(R_{cylinder}^2 - r_{rod}^2\right) \cdot \left[\left(R_{cylinder}^2 - r_{rod}^2\right)(n+1)\right]^n}{\left\{2n\left[((2n+2)/(2n+1))\, R_{piston} \cdot (h/2)^{1/n+2} + (h/2)^{1/n+3} \cdot \left(11n^2+12n+3\right)/(2n+1)(3n+1)\right]\right\}^n} \cdot V^n \tag{44}$$

where $R_{cylinder}$ is the cylinder radius and R_{rod} is the rod radius. The damping coefficientCis defined as

$$C = \frac{2\pi\eta L \cdot \left(R_{cylinder}^2 - r_{rod}^2\right) \cdot \left[\left(R_{cylinder}^2 - r_{rod}^2\right)(n+1)\right]^n}{\left\{2n\left[((2n+2)/(2n+1))\, R_{piston} \cdot (h/2)^{1/n+2} + (h/2)^{1/n+3} \cdot \left(11n^2+12n+3\right)/(2n+1)(3n+1)\right]\right\}^n} \tag{45}$$

Hence, the output damping force can be expressed as

$$F_{DM} = C \cdot V^n \tag{46}$$

4. Computational Parameters

Based on the software of Matlab/Simulink, firstly, the parameters including shock mass m_f and m_v, the kinetic viscosity η, the flow index n, the initial velocity V_0, throttle gap width h, and throttle core shaft length L were imported, then the above motion functions were solved adopting variable step arithmetic according to the fourth-order Runge Kutta method, and the parameters were optimized and corrected. The optimized model could use debugged shock wave simulator for simulating various shock force waves. The specific method was described as follows that practical shock force curve was imported as a known condition; the throttling gap width was derived reversely.

The common velocity of the cannon barrel, the fixed cylinder block; and the moving cylinder block is assumed as V_t; the shock wave curve is finished when the relative velocity is zero.

The kinetic energy theorem for the moving cylinder block is written as

$$m_f V_t = m_f V_0 - \int F_{DM} dt \tag{47}$$

The kinetic energy theorem for the cannon barrel and the moving cylinder block is written as

$$\left(m_C + m_v\right) V_t = m_v V_0 + \int F_{DM} dt \tag{48}$$

The kinetic energy theorem for the cannon barrel, the fixed cylinder block; and the moving cylinder block is written as

$$\left(m_C + m_v\right) V_t + m_f V_t = \left(m_v + m_f\right) V_0 - 0 \tag{49}$$

The shock wave curve was seen as the known condition, the whole impulse was solved using the shock wave curve, then using these input parameters such as the whole impulse, the initial velocity, and the common velocity, the fixed cylinder block mass was solved, and finally, the variable damping gap was derived reversely.

5. Results and Discussions

From the building process of mechanical model, the factors affecting shock wave characteristics were mainly divided into two classes: the first class was the characteristic parameters including the shock mass m_{sm} which was the sum of m_f and m_v, the kinetic viscosity η, the flow index n, and the initial velocity V_0, and the second class was the controlled parameters including throttle gap width h and throttle core shaft length L. The influences of the typical parameters on the shock force wave were analyzed.

5.1. Influence of Different Throttle gap Widths. With the help of the hydraulic cylinder pushing the impact head to achieve the impact on the muzzle by the designed initial impact speed 15ms^{-1}, the shock duration was finished when the relative velocity was equal to zero. For describing the influence of the throttle gap width h of the fluid damping passage on the shock behavior, the shock force wave was simulated under different throttle gap widths h of the fluid damping passage. The curves were shown as Figure 7.

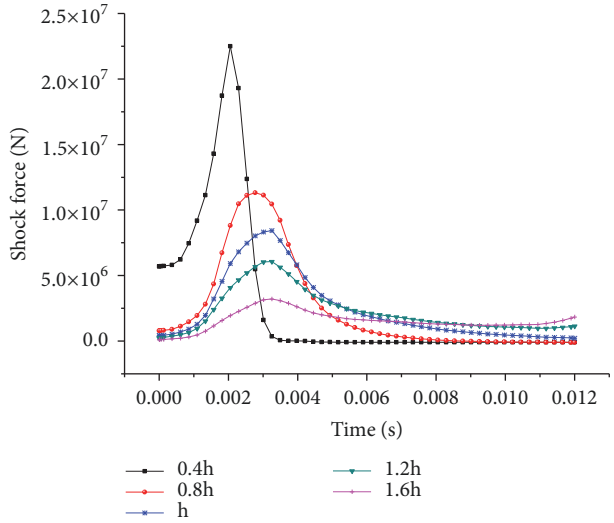

Figure 7: Shock forces under different throttle gap widths.

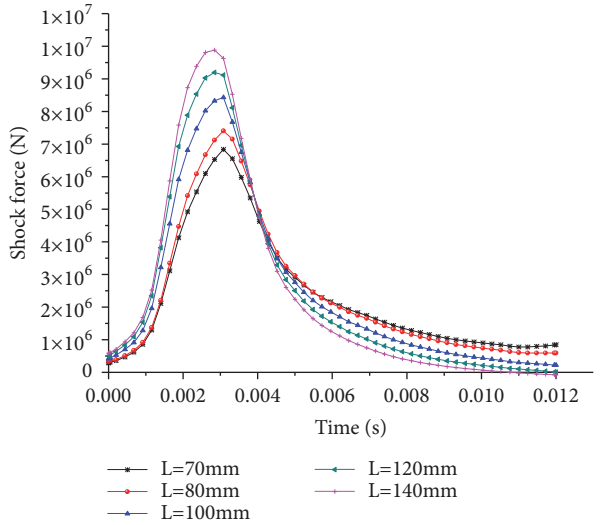

Figure 8: Shock forces under different throttle core shaft lengths.

Based on the mathematical model establishment of the fluid damping channel and the derivation of the output damping force, it was concluded that the throttle gap width h of the fluid throttle passage directly affected the throttled flow In controlled parameters, and the throttle flow increased with the increase of the throttle gap width h of the fluid damping passage according to (40). Obviously, Figure 7 revealed that the peak shock forces increased and the shocking duration decreased with the decrease of the throttle gap width h, which meant the shock wave can be adjusted by changing the throttle gap width.

5.2. Influence of Different Throttle Core Shaft Lengths. In controlled parameters, the throttle core shaft length directly affected the damping coefficient and the damping coefficient increased with the increase of the throttle core shaft length. Shock forces under different throttle core shaft lengths were shown as Figure 8.

For describing the influence of the throttle core shaft length on the shock behavior, the shock force wave was simulated under different throttle core shaft lengths. It was obvious that the peak shock forces increased and the shocking duration decreased with the increase of the throttle core shaft length, which meant the shock wave can be adjusted by changing the throttle core shaft length.

5.3. Influence of Different Fluid Flow Indexes. In characteristic parameters, the related physical parameters of the fluid medium including the flow index were important for the output damping force of the damper according to the derivation of the output damping force. So for describing the influence of the fluid flow index on the shock behavior, the shock forces were simulated under various fluid flow indexes. Shock forces under different fluid flow indexes were shown as Figure 9.

It was obvious that the peak shock forces increased and the shocking duration decreased with the increase of the

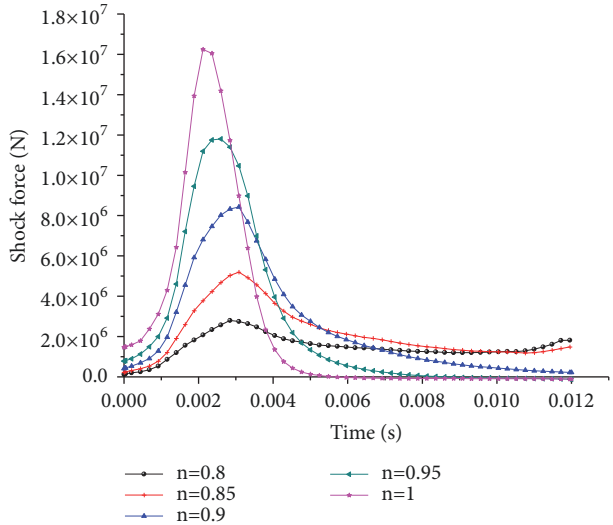

Figure 9: Shock forces under different fluid flow indexes.

fluid flow index, which meant the shock wave was related to the characteristics of the fluid medium and the shock characteristics of the shock wave simulators with variable damping can be adjusted by changing the characteristics of the fluid mediums such as the fluid flow index.

5.4. Shock Wave under Different Velocities. The shock wave characteristics under different impact velocities were also investigated. The computational results under different velocities were shown in Figure 10.

It was obvious that the simulator can satisfy the requirements of different impact velocities. In comparisons, it was obvious that the shape trends of the shock force waves are kept similar under different initial velocities V_0, and the peak value increased with the initial velocity increases, which accorded with the theory analysis as well as the mechanical performances of the shock wave simulator. Just

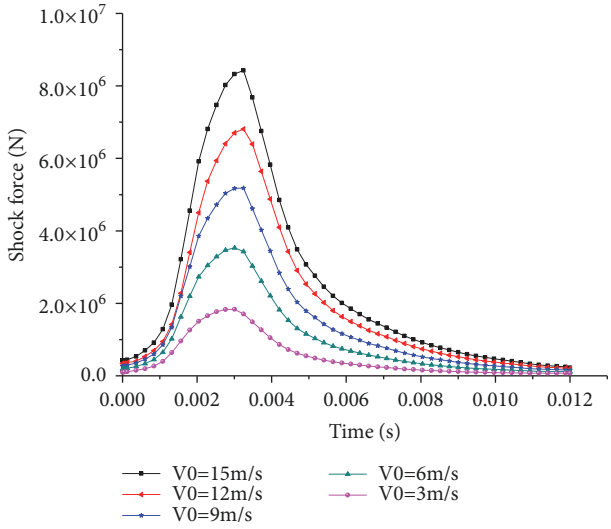

Figure 10: Shock forces under different impact initial velocities.

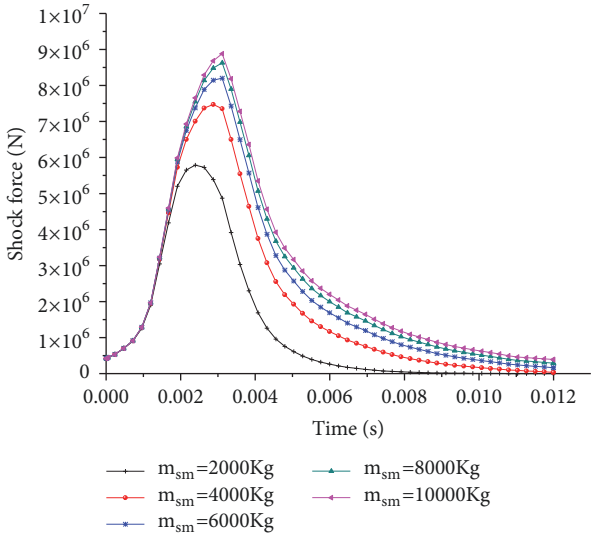

Figure 11: Shock forces under different shock masses.

as shown by the computational results, the shock wave had a little hysteresis, which perhaps was not permitted in some conditions. If this is true, the hysteresis can be attenuated by chamfering the entrance edge of the piston. The angle and the dimension of the chamfer were the important factors for the performance of shock wave. However, in many environments, whether the serious shock wave can be produced was the most important thing, so the hysteresis was not discussed in the paper.

5.5. Shock Wave under Various Shock Masses. In characteristic parameters, for describing the influence of the shock masses on the shock behavior, the shock forces wave was simulated under various shock masses. Shock forces under different shock masses were shown as Figure 11.

It was obvious that the peak shock forces increased and the shock duration increased with the increase of the shock

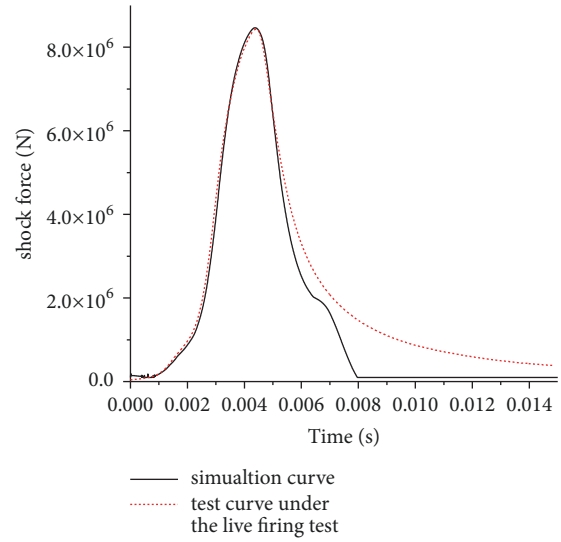

Figure 12: Shock force curves comparison generated by the simulation and the live firing test, respectively.

masses, which meant that the shock wave can be adjusted by changing the characteristics of the input parameters such as the shock masses. Besides, the throttle gap width was obtained by the reverse method that practical shock force curve was imported as a known condition.

The impact initial velocity was $15ms^{-1}$, the shock mass was 6900Kg, the kinetic viscosity was $0.55N{\cdot}s/m^2$, the flow index was 0.9, and throttle core shaft length was 100mm. The shock force wave was simulated adopting the optimized shock parameters in Figure 12. It was indicated that the above mathematical model had good precision by the optimization and the correction of numerical simulation tests under various working conditions, and the variable damping hydraulic shock wave simulator adopting the optimized shock parameters can realize the shock wave reappearance of the shock force on the artillery muzzle in the live firing test.

6. Conclusions

The theoretical analysis and numerical simulation result analysis demonstrated that the variable damping hydraulic shock wave simulator could be used for simulating the shock forces in the cannon recoil motion; the simulation method was reasonable. The working principle of this simulator was explained, the mathematical model was established, and the flow behavior of Newtonian and non-Newtonian fluid in damping channel was analyzed. Finally, the serious shock wave curves were simulated by adjusting the fluid damping parameters, the shock velocity, and the tested mass of novel hydraulic shock wave simulation. The results showed that the shock wave characteristics were directly related to the sectional area of the damping channel and the damping fluid medium characteristic, and the shock wave curve can be simulated by adjusting the variable damping parameters, which meant that the proposed mathematical model can be

used for supplying theoretical references for the cannon recoil motion in artillery fire shock simulation test.

Data Availability

The simulation data used to support the findings of this study are included within the article and the simulation analysis results plots were obtained based on the software Matlab/Simulink.

Conflicts of Interest

The authors declare that there are no conflicts of interest regarding the publication of this paper.

References

[1] M. Cast, "Army test move to 'virtual proving ground'," *National Defence*, vol. 11, pp. 62–64, 2001.

[2] D. Brown, "Simulating firing loads provides flexibility and test repeatability," ADA323489, 1997.

[3] J. Lekan, D. Gotti, A. Jenkins, J. Owens, and M. Johnston, "Users guide for the 2.2 second drop tower of the Nasa Lewis Research Center," *National Aeronautics and Space Administration*, pp. 1–38, 1996.

[4] G. R. Fowles, G. E. Duvall, J. Asay et al., "Gas gun for impact studies," *Review of Scientific Instruments*, vol. 41, no. 7, pp. 984–996, 1970.

[5] "Test operations procedure (TOP): 5-2-521 pyrotechnic shock test procedures," Tech. Rep. TOP 5-2-521, US Army Developmental Test Command, Aberdeen Proving Ground, MD, USA, 2007.

[6] B. Hopkinson, "A Method of Measuring the Pressure Produced in the Detonation of High Explosives or by the Impact of Bullets," *Philosophical Transactions of the Royal Society of London*, vol. 213, no. 612, pp. 437–456, 1914.

[7] M. Gram, A. J. Clark, G. A. Hegemier, and F. Seible, "Laboratory simulation of blast loading on build and bridge structures," *Transactions Built Environment*, vol. 87, pp. 33–44, 2006.

[8] L. K. Stewart, B. Durant, J. Wolfson, and G. A. Hegemier, "Experimentally generated high-g shock loads using Hydraulic Blast Simulator," *International Journal of Impact Engineering*, vol. 69, no. 9, pp. 86–94, 2014.

[9] L. K. Stewart, A. Freidenberg, T. Rodriguez-Nikl et al., "Methodology and validation for blast and shock testing of structures using high-speed hydraulic actuators," *Engineering Structures*, vol. 70, pp. 168–180, 2014.

[10] K. Stewart L, *Testing and Analysis of Structural Steel Columns Subjected to Blast Loads [Dissertations & Theses - Gradworks]*, 2010.

[11] P. Huson, R. J. Asaro, L. Stewart, and G. A. Hegemier, "Non-explosive methods for simulating blast loading of structures with complex geometries," *International Journal of Impact Engineering*, vol. 38, no. 7, pp. 546–557, 2011.

[12] A. Freidenberg, C. W. Lee, B. Durant, V. F. Nesterenko, L. K. Stewart, and G. A. Hegemier, "Characterization of the Blast Simulator elastomer material using a pseudo-elastic rubber model," *International Journal of Impact Engineering*, vol. 60, no. 10, pp. 58–66, 2013.

[13] T. Rodriguez-Nikl, G. A. Hegemier, and F. Seible, "Blast simulator testing of structures: Methodology and validation," *Shock and Vibration*, vol. 18, no. 4, pp. 579–592, 2011.

[14] Y. Yangwu, "Numerical simulations of test system and dynamics of the gun recoil," *Journal of China Ordnance*, vol. 22, no. 2, pp. 152–155, 2001.

[15] X. Hang and Z. Zhang, "Study on dynamic simulation experiments in a artillery dynamic recoil test," *Journal of Ballistic*, vol. 7, no. 1, pp. 29–33, 1995.

[16] D. Changchun, Y. Yuliang, Q. Yuliang, and C. Kaibo, "Research on the effect of shock parameters in a artillery dynamic recoil test device," *Journal of Artillery Launch and Control*, vol. 2, pp. 25–28, 2012.

[17] D. Changchun, L. Lin, Z. Jian, and C. Yongcai, "Numerical analysis of artillery dynamic recoil simulation test based on the principle of artillery muzzle shock," *Combustion, Explosion, and Shock Waves*, vol. 32, no. 3, pp. 323–327, 2012.

[18] Y. Yuliang, Q. Junqi, D. Changchun, and D. Huiyong, "Finite element simulation and test study of the material constitutive model of rubber wave generator," *Mechanical Design*, vol. 30, no. 9, pp. 86–89, 2013.

[19] Y. Yuliang, Q. Junqi, D. Changchun, S. Yezun, and L. Xiaowei, "Accuracy evaluationof artillery dynamic recoil simulation based on numerical and shape similarity," *Journal of Vibration and Shock*, vol. 34, no. 10, pp. 157–160, 2015.

[20] Y. Yuliang, Q. Junqi, D. Changchun et al., "Optimization design of artillery dynamic recoil tester," *Journal of Vibration and Shock*, vol. 33, no. 2, pp. 47–51, 2014.

[21] Y. Yang, C. Changchun, D. Wu et al., "Design on the Theoretical Breechblock Operating Force of Shock Test Bed for artillery Breechblock System," in *Proceedings of the International Conference on Information Engineering for Mechanics and Materials*, 2015.

[22] Y. Yang, J. Zheng, D. Changchun, and J. Chen, "Model and simulation on a shock test bed for artillery breechblock system," in *Proceedings of the International Conference on Information Sciences, Machinery, Materials and Energy*, 2015.

[23] M. Cast, "Army test moves to virtual proving ground," *National Defensemble*, vol. 11, pp. 62–64, 2001.

[24] L. Liu, D. Changchun, P. Baoqing, and Y. Jiajun, "Test design and optimization of artillery simulation firing test," *Journal of Artillery Launch and Control*, vol. 3, pp. 99–102, 2010.

[25] S. Jiao, Y. Wang, L. Zhang, and H. Hua, "Shock wave characteristics of a hydraulic damper for shock test machine," *Mechanical Systems and Signal Processing*, vol. 24, no. 5, pp. 1570–1578, 2010.

[26] S. Duym, R. Stiens, and K. Reybrouck, "Evaluation of shock absorber models," *Vehicle System Dynamics*, vol. 27, no. 2, pp. 109–127, 1997.

[27] M. Shams, R. Ebrahimi, A. Raouh et al., "CFD-FEA analysis of hydraulic shock valve behavior," *International Journal of Automotive Technology*, vol. 8, no. 5, pp. 615–622, 2007.

[28] J. Jiuhong, D. Jianye, W. Yu, and H. Hongxing, "Design method for fluid viscous dampers," *Archive of Applied Mechanics*, vol. 78, no. 9, pp. 737–746, 2008.

[29] C.-Y. Hou, "Fluid dynamics and behavior of nonlinear viscous fluid dampers," *Journal of Structural Engineering*, vol. 134, no. 1, pp. 56–63, 2008.

[30] C.-Y. Hou, "Behavior explanation and a new model for nonlinear viscous fluid dampers with a simple annular orifice," *Archive of Applied Mechanics*, vol. 82, no. 1, pp. 1–12, 2012.

[31] C.-Y. Hou, D.-S. Hsu, Y.-F. Lee, H.-Y. Chen, and J.-D. Lee, "Shear-thinning effects in annular-orifice viscous fluid dampers," *Journal of the Chinese Institute of Engineers*, vol. 30, no. 2, pp. 275–287, 2007.

[32] A. Syrakos, Y. Dimakopoulos, and J. Tsamopoulos, "Theoretical study of the flow in a fluid damper containing high viscosity silicone oil: Effects of shear-thinning and viscoelasticity," *Physics of Fluids*, vol. 30, no. 3, Article ID 030708, 2018.

[33] X. Xu, H. Tao, and J. Han, "Shock Mechanism Analysis and Simulation of High-Power Hydraulic Shock Wave Simulator," *Shock and Vibration*, vol. 2017, Article ID 4361256, 10 pages, 2017.

[34] Z. Hanzhong, *Engineering Fluid Mechanics*, Huazhong University of Science and Technology Press, 2005.

[35] S. Zhongtang and L. Henian, *Non-Newtonian Fluid Mechanics and Its Applications*, Beijing Higher Education Press, 1989.